An overview of EBIT data needed for experiments on laser-produced plasmas[1]

M.B. Schneider, R. Mancini, K. Widmann, K.B. Fournier, G.V. Brown, H.-K. Chung, H.A. Baldis, K. Cone, S.B. Hansen, M.J. May, D. Thorn, and P. Beiersdorfer

Abstract: Data produced by an electron beam ion trap (EBIT) can be crucial for interpreting spectra from plasmas created by long-pulse lasers. Four example spectra are considered: (*i*) the spectra from the hot gold plasma in the laser deposition region of a hot hohlraum, (*ii*) the He-β spectra from an argon-doped imploding core of an inertial confinement fusion capsule, (*iii*) the polarization in spectral lines produced by hot electrons generated by laser-plasma parametric instabilities, and (*iv*) the spectra of the underdense plasma from an aerogel X-ray source. The EBIT data needed for these cases are: (*i*) the line positions for $3 \rightarrow 2$ transitions in open M shell gold ions, (*ii*) the Li-like satellite lines for the K-β transition in open L shell argon ions, (*iii*) the polarization of suitable X-ray lines at 30 keV, and (*iv*) the precise wavelengths of K lines of highly charged Si ions and the precise wavelengths of L and K lines of highly charged Ge ions.

PACS Nos.: 52.25.Os, 52.38.−4, 52.38.Bv, 52.57.−z, 52.57.Fg, 52.59.Px, 52.70.−m 52.70.La

Résumé : Les données produites par un piège ionique à faisceau d'électrons (EBIT) peuvent être très importantes pour interpréter les spectres dans les plasmas créés par de longues pulsations laser. Nous étudions quatre types de spectre : (*i*) le spectre d'un plasma d'or chaud dans la région de déposition d'un corps noir chaud, (*ii*) le spectre He-β du coeur dopé à l'argon en implosion d'une capsule de fusion par confinement inertiel, (*iii*) la polarisation dans les lignes spectrales produite par électrons chauds générés par les instabilités paramétriques d'un plasma laser, (*iv*) le spectre du plasma de faible densité d'une source de rayons-X en aérogel. Les données EBIT nécessaires à cette fin sont : (*i*) la position des lignes pour les transitions $3 \rightarrow 2$ dans les couches M ouvertes d'ions d'or, (*ii*) les lignes satellites de type Li pour la transition K-β dans les couches L ouvertes d'ions d'argon, (*iii*) la polarisation de lignes de rayons-X adéquates à 30 keV, (*iv*) les longueurs d'onde précises des lignes K d'ions Si fortement chargés et les longueurs d'onde précises des lignes L et K d'ions Ge hautement chargés.

[Traduit par la Rédaction]

1. Introduction

X-ray spectroscopy of laser-produced plasmas is a valuable tool for diagnosing plasma conditions such as radiation temperature [1], electron temperature [2, 3], ion temperature [4], and electron density [5]. X-ray spectroscopy may be used to probe hot electrons produced in laser-plasma interactions [3, 6]. The X-ray spectra often contain a very complicated mixture [7, 8] of lines produced by different atomic processes [9] from several ionic species in a complex ionization balance. The measured spectrum is often a superposition of emissions from regions in the plasma with different temperatures and densities. Data from EBIT can help interpret the spectra in several ways: EBIT data can be used to identify the lines and the atomic processes that produce them [10]; EBIT data can help deconvolve different contributions to the profile of a single line [5]; and EBIT data can help characterize the suprathermal electrons produced in the interaction of intense laser beams with plasmas [11].

This paper will focus on the spectroscopy of plasmas formed by long-pulse lasers (pulse length ~1 ns) and moderate laser intensities (10^{14}–10^{16} W/cm^2).

This is a challenging regime for performing careful spectroscopy because of the short time duration of the experiment, the high brightness of the plasmas, and the gradients in the plasmas. In addition, X-ray spectroscopy of laser-produced plasmas often sacrifices absolute calibration for time and space information. The dispersive elements used in the spectrometers are similar to those used at EBIT, but the time-resolved detectors are not. These detectors can receive hundreds of photons in a very short time. Detectors include static ones (film, image plates, X-ray CCDs) that can be absolutely calibrated photometrically and have a high dynamic range, but have no temporal information. The two most popular detectors for temporally resolved measurements are X-ray streak cameras [12] and X-ray framing cameras [13]. The X-ray streak cameras have low dynamic range and no spatial information but afford a temporal resolution of better than 30 ps. The X-ray framing cameras can give snapshots of spectra with ~200 ps time resolution and one-dimensional imaging information. They have a dynamic range

Received 2 July 2007. Accepted 11 September 2007. Published on the NRC Research Press Web site at http://cjp.nrc.ca/ on 9 February 2008.

M.B. Schneider,[2] K. Widmann, K.B. Fournier, G.V. Brown, H.-K. Chung, S.B. Hansen, M.J. May, and P. Beiersdorfer. Lawrence Livermore National Laboratory, P.O. Box 808, Livermore, CA 94550, USA.
R. Mancini. Deparment of Physics, University of Nevada, Reno, Nevada 89557, USA.
H.A. Baldis, K. Cone, and D. Thorn. Department of Applied Science, University of California, Davis, CA 95616, USA.

[1] Paper given at the Workshop on Twenty Years of Spectroscopy with EBIT held in Berkeley, California, 13–15 November 2006.
[2] Corresponding author (e-mail: schneider5@llnl.gov).

 doi: 10.1139/P07-179

of ∼300. However, the gain of the framing camera can vary by as much as a factor of three across the spectrum, so the gain must be measured and the spectra must be corrected for it [14].

EBIT measurements can fill essential needs of these experiments. They can characterize and calibrate the dispersive elements of the spectrometers.[3] EBIT can be used to measure the positions of lines corresponding to the same type of transition in different charge states. EBIT can be used to measure contributions to the linewidth that arise from different excited states of the same ion. EBIT can also be used to measure the polarizations of a given line. EBIT measurements can accurately determine the positions of the K and L shell lines of a given species and of a mixture of species. The EBIT experiments help identify unknown features in the emission spectrum of laser-produced plasmas and also benchmark the theoretical calculations used to model the laser-produced plasmas.

This paper focuses on four examples where EBIT data are used or are needed to successfully interpret data from laser-produced plasmas. The first example is the hot non-LTE (local thermodynamic equilibrium) gold plasma in the laser deposition region of a hot hohlraum. The $3 \rightarrow 2$ lines of open M shell gold ions can be used to deduce the electron temperature, T_e. The second example is an imploding capsule similar to those used in inertial confinement fusion (ICF). (The capsule is doped with Ar, and the shape of the Ar He-β line is fitted to deduce T_e and the electron density, n_e, as a function of time.) The third example is a proposed experiment to measure properties of the hot electrons generated by laser-plasma instabilities. The polarization of an X-ray line at 30 keV would be a sensitive measure of the directionality of the hot electrons. And finally, the fourth example is the characterization of the underdense plasma of a newly developed X-ray source, silica aerogel doped with germanium. The region of the K line emission of silicon is filled with many satellite lines of Si, many L lines of Ge, and higher order Ge K lines. These lines must be identified.

1.1. Line identification of the $3 \rightarrow 2p$ transitions near 10 keV in open M shell gold ions

Spectrometers often look at the emission spectrum of a single element in a plasma to measure its charge state distribution. The charge state distribution can be compared to those predicted by collisional-radiative atomic physics codes, such as FLYCHK [15] and SCRAM [16], to deduce T_e. This is true if the electron density n_e is known or if the spectrum is insensitive to n_e. The spectrum has a "picket-fence" appearance because of numerous almost equally spaced lines from the same type of transition repeated in ions of different charge. The example discussed here is the spectrum of the $3 \rightarrow 2$ transitions in the 10 keV X-ray range in an open M shell gold plasma (Widmann [17]). The gold plasma is in the laser deposition region of a hot hohlraum [18].

High-temperature ("hot") hohlraums [18, 19] are being developed as thermal X radiation sources for radiation-heating experiments at the OMEGA [20] and National Ignition Facility (NIF) [21] lasers. Figure 1 shows a typical hot hohlraum target. It is a small (400–800 μm diameter) hollow gold cylinder with an open end to allow the laser beams to enter and a closed end, referred to as the "back wall". The hohlraum is heated by up to 9.5 kJ of energy using about 20 laser beams in a 1 ns long-pulse of 351 nm light. The laser beams deposit their energy in the plasma formed inside the hohlraum by hot wall material ablating into the hohlraum. The electrons in the plasma absorb the laser energy via inverse bremsstrahlung interactions. The energy from the electrons is conducted to hohlraum walls which are near the laser deposition (laser spot) region, and these walls emit X-rays. The X-rays are then absorbed and remitted by all of the walls of the hohlraum, thereby heating the walls and "thermalizing" the X-ray spectra. Ideally, the plasma remains near the walls, the areas of the laser "spots" are small compared to the total wall area, and the cavity remains empty. In this ideal picture, hohlraums are "blackbody-like" X radiation sources [22–25].

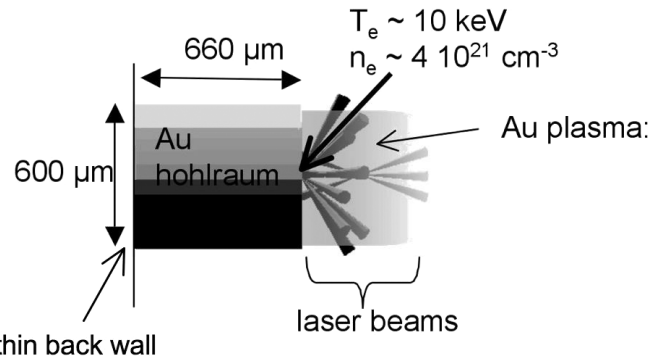

Fig. 1. Geometry of the hot hohlraum experiment at the OMEGA laser. The hohlraum is a small gold cylinder with a thin back wall. Late in time, gold plasma has filled the hohlraum, and the plasma in which the lasers deposit their energy has moved to the front of the hohlraum where the laser beams enter. The gold plasma here is very hot. The plasma conditions are quasi-steady state after the laser has been on for about 0.7 ns [19].

Unlike conventional hohlraums [22–25], the hot hohlraums are so small that they are mainly "laser spots". This is because the gold plasma ablated from the hot walls quickly fills the hohlraum [18, 19], and during the second half of the laser pulse the laser is depositing its energy in the plasma at the front entrance of the hohlraum. After the laser has been turned on for ∼0.5 ns, the hot hohlraum has filled to an electron density $n_e \sim 0.4 n_c$ (4×10^{21}/cm^3) and higher, where n_c is the critical density, the density at which light can no longer propagate. For 351 nm light, $n_c = 9 \times 10^{21}$/cm^3. After the laser has been turned on for about 0.7 ns, the plasma conditions in the laser deposition region at the entrance to the hohlraum are in a quasi-steady state [19].

The plasma in the laser deposition region in the quasi-steady state phase is predicted to have a high T_e (10–12 keV) [19, 26]. The L-band spectrometer was built to measure the $2p_{1/2}^2 2p_{3/2}^3 3s^k 3p^{k'} 3d^{k''} 3d_{5/2} \rightarrow 2p^6 3s^k 3p^{k'} 3d^{k''}$ transitions near 10 keV of the gold ions in this plasma with enough resolution to see lines from individual ions, and thus directly measure the charge state distribution. Theoretical models use the charge state distribution to deduce T_e.

The L-band spectrometer is a transmission crystal spectrometer [17]. It is designed to have a resolution of 15 eV and to record the spectral region from 9.5 to 10.5 keV. This matches the energy region of the transitions in gold. The spectrometer is mated to a single-strip X-ray framing camera [13, 14] so the spectrum is a "snapshot" with an 80 ps window. The data are

[3] K. Widmann. Private communication. 2007.

Fig. 2. (*a*) High-resolution emission spectra from the laser deposition region of a hot hohlraum (Fig. 1) late in time (∼0.9 ns). The spectrometer was looking into the hohlraum at a 63° angle to the to axis of the hohlraum. The LEH looked elliptical in this view, and the spectral direction was along the long axis of the ellipse (perpendicular to the hohlraum axis). The L band spectrometer is designed to look at $3d_{5/2} \rightarrow 2p_{3/2}$ X-ray lines with a resolution of ∼15 eV (Widmann et al. [17]). (*b*) Modeled spectra as a function of T_e for $n_e = 1 \times 10^{21}/cm^3$ using FLYCHK for the charge state distribution and FLYSPEC for spectra (Chung et al. [15]. The picket-fence pattern of lines shifts to higher X-ray energy at a rate of ∼70 eV per 1 keV in T_e.

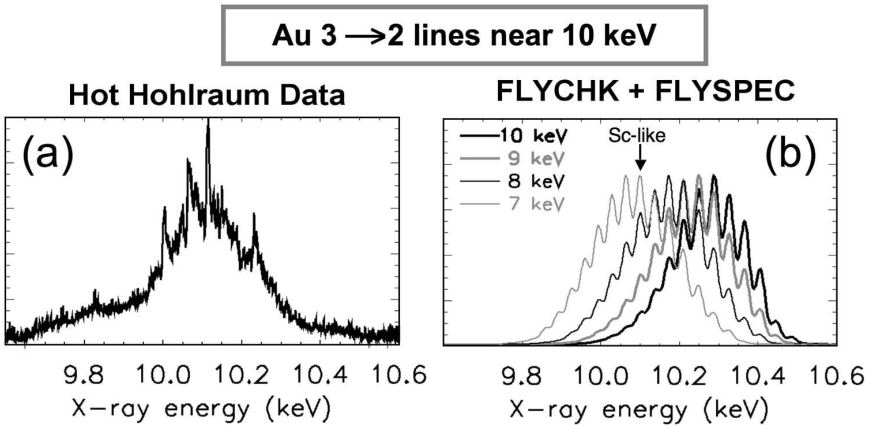

an image, with spectra in one direction and spatial information in the other. A lineout of the data through the laser deposition region is shown in Fig. 2*a*. This spectrum was taken during the steady-state phase at about 0.9 ns.

To deduce T_e, the measured spectrum must be compared with theory. FLYCHK [15] was used to model the charge state distribution for a uniform gold plasma with a density of $\sim 10^{21}/cm^3$ as a function of electron temperature. The FLYSPEC code took this distribution and calculated the spectra for the different electron temperatures. The results, after the spectra were normalized to the same value for display purposes, are shown in Fig. 2*b*. For each temperature, the spectrum is a picket-fence of lines, as mentioned earlier. The centroid of the distribution of the lines and the distribution itself are sensitive to the electron temperature [2]. FLYCHK predicts that the effective charge $< Z >$ is relatively insensitive to n_e in this range [2]. The lines from the different charge states of Au are separated by about 40 eV. As Fig. 2*b* shows, a 40 eV shift in the calibration of the energy scale thus corresponds to a ∼600 eV shift in T_e.

Accurate line positions for the Au $3 \rightarrow 2$ emission lines near 10 keV are necessary to reliably model the spectrum from gold laser-produced plasmas. The position of each line from each charge state must be correctly identified. The data in Fig. 2*a* have a mean charge state that is roughly Sc- or Ca-like, corresponding to a line-of-sight averaged electron temperature between 7 and 8 keV. This is lower than would be the case if the plasma were as hot as predicted [2, 19]. EBIT can be used to unambiguously identify the lines from the different charge states. Figure 3 shows existing EBIT data. Also indicated are some Hebrew University Lawrence Livermore atomic code (HULLAC) [27] positions for several lines. They agree for the line positions of the more highly charged gold ions, but there may be some disagreement for the line positions of the less highly charged gold ions. More EBIT data are needed — because the data from the laser-produced plasma are centered around lower charge states than originally predicted. EBIT data need to be recorded for lower charge states than the data shown in Fig. 3. In addition, temperature and density gradients along the line-of-sight must be considered in the interpretation of the data.

Fig. 3. EBIT data for $3 \rightarrow 2$ transitions near 10 keV in Au. (Widmann et al. [17]) The different charge states are labeled. Also shown are HULLAC calculations (May et al. [2]) for the line positions.

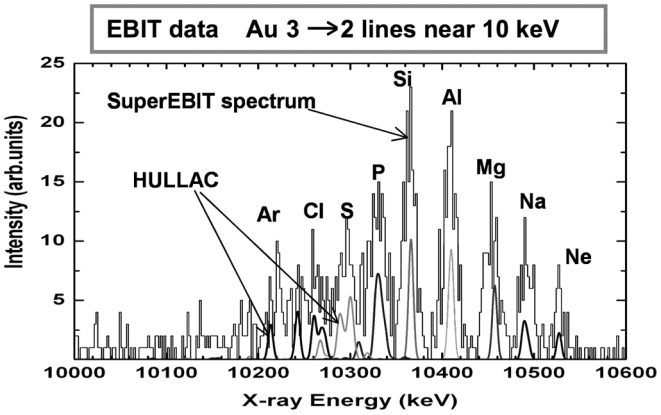

For completeness, we mention that laser-produced Au plasmas at lower temperatures ($T_e \sim 2$–3 keV) have been studied with Au M shell spectroscopy [7, 28–30]. May et al. [7, 31], have compared Au plasma M shell spectroscopy from EBIT, HULLAC modeling, and laser-produced plasmas.

1.2. Line broadening of the Ar He-β line

X-ray spectroscopy of inertial confinement fusion (ICF) implosion cores is a useful diagnostic of fuel temperature and density conditions. An ICF capsule can be imploded by direct heating with laser beams or by indirect heating with X-rays, whose energy comes from laser beams. Knowledge of the density of the imploding capsule as a function of time is crucial to understand the implosion dynamics. If some argon is mixed with the core gas, then the linewidth of the Ar He-β line can be used to deduce the electron temperature and density of the

Fig. 4. Indirect drive inertial confinement fusion implosion experiment. (*a*) Geometry of the imploding core experiment at NOVA. (Woolsey et al. [33]); laser energy is converted to X-ray energy in the hohlraum. The X-ray drive from the hohlraum heats the outside of the microsphere (the imploding core). The ablation of the heated material on its outside causes the microsphere to implode. (*b*) Schematic of the microsphere. The low-Z gas fill is doped with argon.

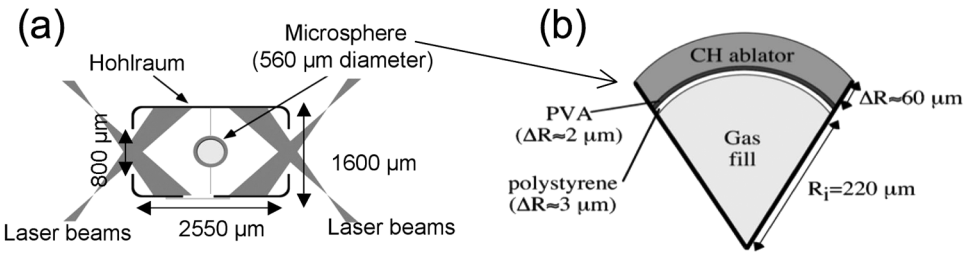

imploding core (Golovkin and Mancini [32]). Figure 4 shows an indirect-drive target used to simulate the implosion of an ICF capusule [33].

The density and temperature can be measured spectroscopically by measuring the linewidth of a Stark-broadened line [34]. To this end, the deuterium gas fill is doped with a small amount of a suitable tracer element whose X-ray line emission is recorded at the collapse of the implosion using streaked crystal spectrometers [35]. The selection of the tracer element depends on the deuterium plasma conditions to be diagnosed. For implosion cores that typically achieve electron number densities of order $10^{24}/\text{cm}^3$ and electron temperatures of about 1 keV, argon is a good choice since it becomes highly ionized and emits K shell lines from Li-, He-, and H-like ions, which yield a line spectrum rich in information about plasma environmental conditions. We note in passing that the electron number density of argon-doped deuterium plasmas is approximately equal to the deuterium atom number density (and thus the mass density) since the population of free electrons is dominated by the ionization of deuterium. The information is encoded in the line intensities, which are sensitive to electron temperature and density through the collisional-radiative atomic kinetics and level population distribution and the line broadening that is mainly dependent on density via the Stark broadening effect.

The He-β $1s3p \rightarrow 1s^2$ line transition in He-like Ar represents an interesting choice for plasma diagnostics. On the one hand, it is less optically thick than the He-α $1s2p \rightarrow 1s^2$ line but still bright enough for meaningful analysis. On the other hand, for the same plasma conditions the Stark broadening of the He-β line is larger than that of the He-α line, which makes it suitable for a density diagnostic. Furthermore, it was pointed out that in the hot dense plasmas of implosion cores, significant satellite line emission from $n = 3 \rightarrow 1$ transitions in Li-like Ar blends with the He-β line, thus giving rise to a composite spectral feature that is sensitive to both temperature and density [35].

The line intensity distribution of Stark-broadened $1s3pnl \rightarrow 1s^2nl$ line transitions with $n \geq 2$ in Li-like Ar ions spreads over a significant photon energy range from the low-energy wing to the core of the He-β line, thus significantly overlapping with this line. As the plasma temperature and density conditions change so do relative intensities and broadening, thus producing varying levels of blending with He-β, including a significant change in the linewidth. Detailed modeling of the He-β composite spectral feature in argon yields a temperature and density dependent line spectrum that covers the photon energy range from 3550 to 3750 eV [32]. Accurate detailed modeling is important for the quality of the diagnostic application and depends critically on high-quality atomic data including line locations and dielectronic recombination rates. In this connection, data from argon He-β and associated Li-like satellite line spectra recorded at EBIT experiments have been important for the development and testing of atomic models of this composite spectral feature [36].

Fig. 5. (*a*) Synthetic argon He-β composite spectral feature for conditions relevant to implosion core hot dense plasma (Golovkin et al. [32]). The composite spectrum shows the apparent increase in the He-β linewidth due to the blending with Li-like satellite emission. (*b*) Selective excitation of the Li-like dielectronic satellite to the He-β line using EBIT (Smith et al. [36]). Accurate measurement of relative line transition location is important for modeling of the He-β composite spectral feature.

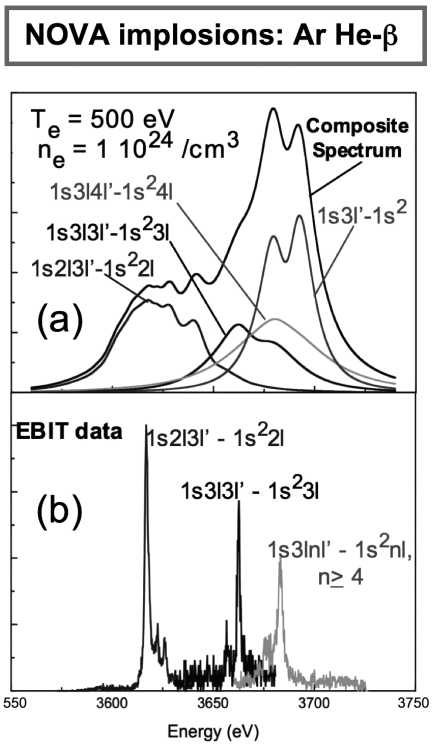

Figure 5*b* displays a dielectronic satellite line spectrum due to Li-like Ar $1s3pnl \rightarrow 1s^2nl$ line transitions with $n \geq 2$ recorded at EBIT, where the electron beam energy was carefully

Fig. 6. (*a–c*) Analysis of a sequence of time-resolved line spectra from the NOVA experiment. The temperature and density dependence of the argon He-β composite spectral feature permits the extraction of the time history of the core's plasma conditions at the collapse of the implosion (Golovkin [38]).

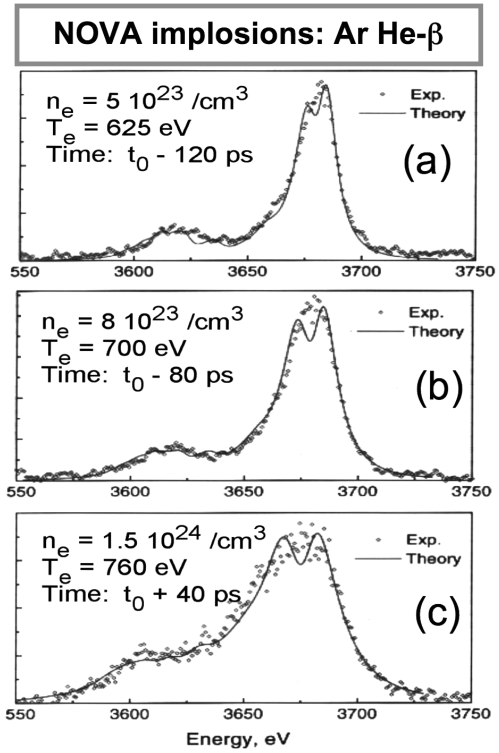

scanned to selectively excite satellite lines for different values of the principal quantum number n of the spectator electron [36]. The EBIT data clearly show the relative location of several types of satellite line transitions and the shift of the satellite emission as n increases. In the EBIT experiment, these satellite transitions are excited by dielectronic recombination. In the hot dense plasmas of implosion cores innershell collisional excitation and collisional mixing among autoionizing states are also important for the level population kinetics; in addition, the line shapes are broadened by the Stark effect due to the plasma microfields. The benchmarking of theoretical atomic data with EBIT experiments is crucial for the quality of spectral modeling. Shown in Fig. 5*a* is a synthetic calculation for $T_e = 500$ eV and $n_e = 1 \times 10^{24}/\text{cm}^3$ that includes relevant atomic kinetics and broadening effects for the implosion core plasma [32]. The effect of the blending in the overall (envelope) line intensity distribution of satellite and He-β emissions is clearly illustrated as well as the break down in individual contributions. The left side of the line (3550 to ~3650 eV) is sensitive to T_e, since it contains contributions from the Li-like charge state. The right side of the lineshape is more sensitive to n_e, since it is mainly the He-β line.

Figures 6*a*–6*c* show the application of the temperature and density dependence of the argon He-β composite spectral feature to the spectroscopic diagnosis of implosion core conditions. The data were recorded at the collapse of indirect-drive implosion experiments performed at the NOVA [37] laser using 440 μm diameter plastic shells filled with 50 atm (1 atm = 101.325 kPa) of deuterium and 0.1 atm of argon [33].

Fig. 7. (*a*) and (*b*) Polarization measurements of He-like and Li-like Ti using a crystal spectrometer at EBIT (Beiersdorfer et al. [11]). The crystal used and the Bragg angle are stated in the figures. The lines w and q have the greatest positive polarization; the line x has the greatest negative polarization.

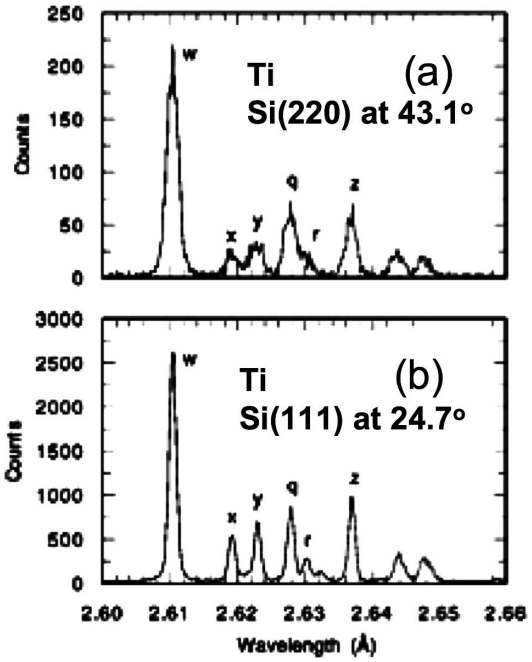

Fig. 8. Schematic diagram of an experiment to measure the directionality of the hot electrons generated in laser-plasma parametric instabilities. One spectrometer is along the laser beam axis, one spectrometer is perpendicular to the laser beam axis. The temperature of the hot electrons is >30 keV [26, 40, 47].

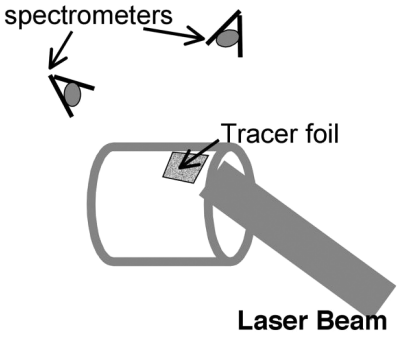

As the implosion core goes through the final phase of the implosion, the intensity distribution changes in shape and broadens; detailed analysis of each time-resolved line spectrum yields a time history of spatially-averaged temperature and density in the core [38]. Finally, we note that the impact of the detailed modeling of the argon He-β spectral feature goes beyond space-averaged spectroscopic analysis. Indeed, it is also important for extracting the spatial profiles of the temperature and density in the core since those are used in the analysis to constrain the possible range of values for the density [39].

1.3. X-ray line polarization measurements as a diagnostic

X-ray lines emitted from a plasma are polarized if there is a symmetry-breaking mechanism that defines a special axis, for

Fig. 9. (*a*) Geometry of the aerogel target at the OMEGA laser (Fournier et al. [48, 49]). The target is a Be cylinder filled with Ge-doped silica aerogel. Forty laser beams with a 1 ns pulse length heat the target. (*b*) Time integrated X-ray pinhole image of the aerogel target showing that the entire volume is emitting.

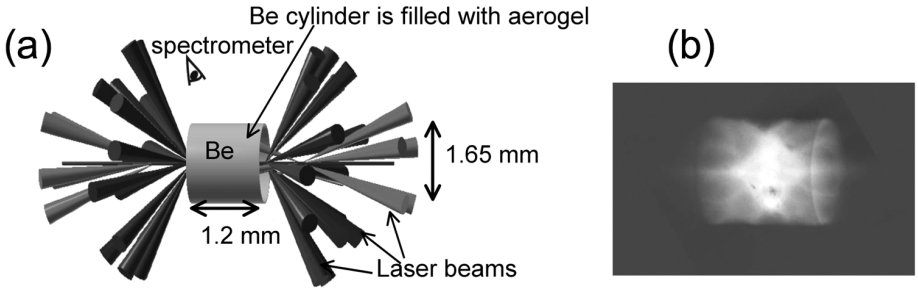

example, a magnetic field, an electric field, or an anisotropic electron distribution. Measuring the polarization of X-ray lines can be a useful diagnostic to detect hot electrons produced in nonthermal processes. Parametric instabilities in laser-plasma interactions can produce a flux of anisotropic "suprathermal" electrons [3, 24, 26, 40]. The directionality of these electrons could be detected in an experiment that measures the polarization of a suitable X-ray line.

Models that can predict line polarizations must be developed. X-ray line polarization measurements at EBIT were useful to guide the development of magnetic sublevel atomic kinetics models. EBIT data have been used to benchmark models for He-like Sc [41, 42], He-like Ti [11], Li- and Be-like Fe [43, 44] , and B-like Fe [45]. These studies were begun to explain the line emission from high-intensity, sub-ps laser-produced plasmas [6, 46]. Figure 7 shows the EBIT measurement for He-like Ti.

Plasmas produced by long-pulse lasers may also have an anisotropic electron distribution. Some resonant instabilities from laser-plasma interactions, such as stimulated Raman backscattering or stimulated Raman forward scattering can produce very hot electrons [26, 40] that are believed to be directional. These suprathermal electrons have not been directly detected. The suprathermal electrons are indirectly detected by measuring the bremsstrahlung radiation from their interaction with the gold walls of the hohlraum. The hard X-ray flux generated by the bremsstrahlung is measured with low-resolution X-ray spectrometers [47].

A geometry such as that shown in Fig. 8 could be used to directly detect the electrons by measuring the polarization of lines emitted by a test foil. The choice of test foil material would have to be matched to the suprathermal electron temperature, which is 30 keV [47] or higher [26]. The suprathermal electrons must be able to excite K shell transitions in the test foil. The modeling of line polarizations would have to be extended to X-ray lines around 30 keV, and EBIT measurements would be needed to benchmark the codes. EBIT would also be needed to calibrate the polarization spectrometers.

1.4. Transition energies of Si K and Ge L lines from Ge-doped silica aerogel plasmas

Bright, multi-keV X-ray sources are needed as backlighters for imaging very large or very dense targets. An example is the implosion core of an ICF target at the NIF. The implosion core is large and dense enough to entirely absorb sub-keV X-rays. Ideally, the source used as the backlighter would have a relatively narrow spectral bandwidth in the hard X-ray spectral region so that the target can be doped with a selected absorbing material. For example, the X-ray energy range is chosen such that the X-rays are transmitted through a background plasma (such as ablated hohlraum material) but are absorbed by the object of interest (such as one of the thin shells in an imploding capsule). The Ge-doped silica aerogel sources developed by Fournier et al. [48, 49] are bright, multi-keV, narrow bandwidth sources and would be ideal candidates for these backlighters.

Figure 9*a* shows the geometry of the aerogel source, as fielded at the OMEGA laser. Aerogels are used to keep the electron density roughly constant at a density below the critical density. Under these conditions, the laser beam deposits its energy in the entire volume. The silica aerogel is doped with Ge to define the source bandwidth as the K emission region of He-like Ge. Figure 9*b* is a hard X-ray image of the source, showing that the entire volume is emitting X-rays. Figure 10 shows the source spectrum. In order to maximize the conversion of laser light to He-like Ge X-rays, the mass density, laser illumination, geometry, and doping levels must be tuned. The simulations of this target must be compared to measurements of plasma conditions. X-ray spectroscopy of the silicon is a valuable tool for this.

Figure 11 shows a time-and-space integrated spectrum in the X-ray region of the He- and H-like Si emission. The spectrum was obtained with a crystal spectrometer [50]. The spectrum is rich with satellite lines. It also contains Ge L lines, and it is contaminated with higher order (4th and 5th order) Ge K lines, making the interpretation of the spectrum more challenging. This is a non-LTE plasma and much plasma information is in the Si satellite lines. EBIT data are needed to identify the silicon and Ge lines. It is important to have a measurement of the line positions because previous EBIT measurements have shown theoretical line positions can be inaccurate [51].

2. Summary

EBIT data are needed to support experiments on laser-produced plasmas. Four examples have been discussed.

(*i*)The electron temperature in the laser deposition region of a hot hohlraum can be measured with high-resolution spectroscopy of the $3d_{5/2} \rightarrow 2p_{3/2}$ transitions in an open M shell gold plasma. The measurements are centered around Ca-like

Fig. 10. Spectrum of the hard X-rays showing that the source is narrow band and bright.

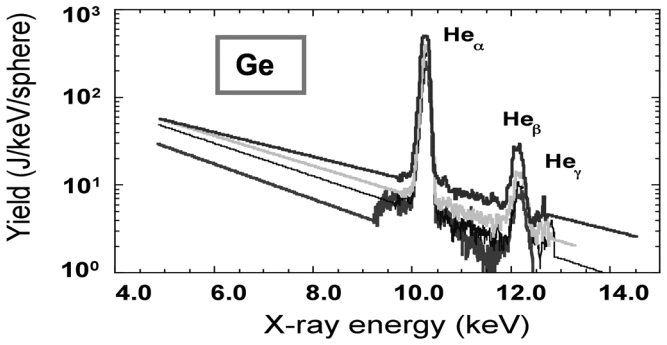

Fig. 11. Spectrum in the Si K X-ray range taken with a time-and-space integrated crystal spectrometer. There are an abundance of Si K satellite lines, some Ge L lines, and higher order (4,5) Ge K lines.

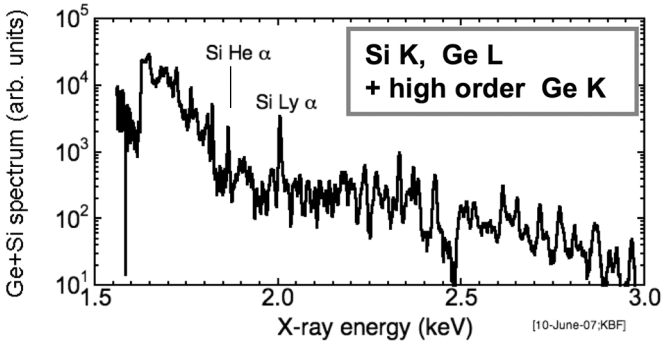

or Sc-like Au. EBIT is needed to measure the Au line positions in this region because one charge state is a ∼600 eV shift in T_e.

(*ii*)EBIT data on the position of satellite lines of Li-like and He-like Ar were used in models of the Ar He-β lineshape of an imploding ICF capsule. This allowed T_e and n_e as a function of time to be measured from the line shape. Similar data may be needed for the He-β satellites of higher Z elements as higher temperatures are achieved on the NIF. Kr may replace Ar in some future experiments [52].

(*iii*)EBIT has been used to measure line polarizations. Parametric laser-plasma instabilities can produce anisotropic suprathermal electrons. A polarization measurement at 30 keV could detect these electrons if a suitable line can be found.

(*iv*)EBIT measurements are needed to identify the Si K lines and the Ge L and K lines in the underdense plasma of a Ge-doped silica aerogel to deduce the plasma conditions and compare the results to predictions from theory.

As these examples show, spectroscopy is an important diagnostic of long-pulse laser experiments. Accurate atomic data are clearly needed to properly utilize this diagnostic and to extract reliable information on the plasma conditions. EBIT can provide much of the needed data and thus can play a major supporting role in understanding laser-produced plasmas.

Acknowledgements

This work performed under the auspices of the US Department of Energy by Lawrence Livermore National Laboratory in part under Contract W-7405-Eng-48 and in part under Contract DE-AC52-07NA27344, by the University of California, Davis under grant number DE-FG52-2005NA26017 (NLUF), and University of Nevada, Reno under grant number DE-FG52-03SF22696 (Mancini - NLUF).

References

1. H.N. Kornblum, R.L. Kauffman, and J.A. Smith. Rev. Sci. Instrum. **57**, 2179 (1986)
2. M.J. May, M.B. Schneider, H.-K. Chung, and D.E. Hinkel. Lawrence Livermore National Laboratory Rep. No. UCRL-JRNL-214752 (2005).
3. S.H. Glenzer, F.B. Rosmej, R.W. Lee, C.A. Back, K.G. Estabrook, B.J. MacGowan, T.D. Shepard, and R.E. Turner. Phys. Rev. Lett. **81**, 365 (1998).
4. V.V. Gavrilov, A.Yu. Gol'tsov, N.G. Koval'skii, S.N. Koptyaev, A.I. Magunov, T.A. Pikuz, I.Yu. Skobelev, and A.Ya. Faenov. Quantum Electron. **31**(12), 1071 (2001).
5. N.C. Woolsey, B.A. Hammel, C.J. Keane, A. Asfaw, C.A. Back, J.C. Moreno, J.K. Nash, A. Calisti, C. Mosse, R. Stamm, B. Talin, L. Klein, and R.W. Lee. Phys. Rev. E, **56**, 2314 (1997).
6. J.C. Kieffer, J.P. Matte, M. Chaker, Y. Beaudoin, C.Y. Chien, S. Coe, G. Mourou, J. Dubau, and M.K. Inal. Phys. Rev. E, **48**, 4658 (1993).
7. M.J. May, P. Beiersdorfer, M. Schneider, S. Terracol, K.L. Wong, K. Fournier, B. Wilson, J.H. Scofield, K.J. Reed, G. Brown, F.S. Porter, R. Kelley, C.A. Kilbourne, and K.R. Boyce. AIP Conf. Proc. **730**, 6172 (2004).
8. R. Shepherd, P. Audebert, H-K Chung, K.B. Fournier, O. Peyreusse, S. Moon, R.W. Lee, D. Price, L. Klein, J.C. Gauthier, and P. Springer. J. Quant. Spectrosc. Radiat. Transfer, **81**, 431 (2003).
9. M.E. Foord, S.H. Glenzer, R.S. Thoe, K.L. Wong, K.B. Fournier, B.G. Wilson, and P.T. Springer. Phys. Rev. Lett. **85**, 992 (2000).
10. K.B. Fournier, M.E. Foord, B.G. Wilson, S.H. Glenzer K.L. Wong, R.S. Thoe, P. Beiersdorfer, and P.T. Springer. AIP Conf. Proc. **547**, 203 (2004).
11. P. Beiersdorfer, G. Brown, S. Utter, P. Neill, K.J. Reed, A.J. Smith, and R.S. Thoe. Phys. Rev. A, **60**, 4156 (1999).
12. D.H. Kalantar, P.M. Bell, R.L. Costa, B.A. Hammel, O.L. Landen, T.J. Orzechowski, J.D. Hares, and A.K.L. Dymoke-Bradshaw. Lawrence Livermore National Laboratory Rep. No. UCRL-JRNL-123776 (1996).
13. K.S. Budil, T.S. Perry, P.M. Bell, J.D. Hares, P.L. Millter, T.A. Peyser, R. Wallace, H. Louis, and D.E. Smith. Rev. Sci. Instrum. **67**, 485 (1996).
14. O.L. Landen, P.M. Bell, J.A. Oertel, J.J. Satariano, and D.K. Bradley. Lawrence Livermore National Laboratory Rep. No. UCRL-JRNL-112384 (1994).
15. H.-K. Chung, M.H. Chen, W.L. Morgan, Y. Ralchenko, and R.W. Lee. High Energy Density Phys. **1**, 3 (2005).
16. S.B. Hansen, A.S. Shlyaptseva, A.Y. Faenov, I.Y. Skobelev, A.I. Magunov, T.A. Pikuz, F. Blasco, F. Dorchies, C. Stenz, F. Salin, T. Auguste, S. Dobosz, P. Monot, P. D'Oliveira, S. Hulin, U.I. Safronova, and K.B. Fournier. Phys. Rev. E, **66**, 046412 (2002).

17. K. Widmann, M.B. Schneider, G.V. Brown. Bull. Am. Phys. Soc. DPP06 NP1.00147 (2006).
18. D.E. Hinkel, M.B. Schneider, B.K. Young, A.B. Langdon, E.A. Williams, M.D. Rosen, and L.J. Suter. Phys. Rev. Lett. **96**, 195001 (2006).
19. M.B. Schneider, D.E. Hinkel, O.L. Landen, R. Bahr, H.A. Baldis, C. Constantin, V. Glebov, R.F. Heeter, A.B. Langdon, M.J. May, J. McDonald, W. Seka, M. Singh, C. Stoeckl, L.J. Suter, K. Widmann, and B.K. Young. Phys. Plasmas, **13**, 112701 (2005).
20. T.R. Boehly, R.S. Craxton, T.H. Hinterman, J.H. Kelly, T.J. Kessler, S.A. Kumpan, S.A. Letzring, R.L. McCrory, S.F.B. Morse, W. Seka, S. Skupsky, J.M. Soures, and C.P. Verdon. Rev. Sci. Instrum. **66**, 508 (1995).
21. G.H. Miller, E.I. Moses, and C.R. Wuest. Nucl. Fusion, **44** S228 (2004).
22. R. Sigel, S. Pakula, S. Sakabe, and G.D. Tsakiris. Phys. Rev. A, **38**, 5779 (1988).
23. R.L. Kauffman, L.J. Suter, C.B. Darrow, J.D. Kilkenny, H.N. Kornblum, D.S. Montgomergy, D.W. Phillion, M.D. Rosen, A.R. Theissen, R.J. Wallace, and F. Ze. Phys. Rev. Lett. **73**, 2320 (1994).
24. J. Lindl. Phys. Plasmas, **2**, 3933 (1995).
25. L.J. Suter, R.L. Kauffman, C.B. Darrow, A.A. Hauer, H. Kornblum, O.L. Landen, T.J. Orzechowski, D.W. Phillion, J.L. Porter, L.V. Powers, A. Richard, M.D. Rosen, A.R. Thiessen, and R. Wallace. Phys. Plasmas, **3**, 2057 (1996).
26. A.B. Langdon and D.E. Hinkel. Phys. Rev. Lett. **89**, 015003 (2002).
27. A. Bar-Shalom, M. Klapisch, and J. Oreg. J. Quant. Spectrosc. Radiat. Transfer, **71**, 169 (2001).
28. M.E. Foord, S.H. Glenzer, R.S. Thoe, K.L. Wong, K.B. Fournier, B.G. Wilson, and P.T. Springer. Phys. Rev. Lett. **85**, 992 (2000).
29. R.F. Heeter, S.B. Hansen, P. Beiersdorfer, M.E. Foord, K.B. Fournier, D.H. Froula, A.J. Mackinnon, M.J. May, M.B. Schneider, and B.K.F. Young. AIP Conf. Proc. **730**, 103 (2004).
30. R.F. Heeter, S.B. Hansen, K.B. Founier, M.E. Foord, D.H. Froula, A.J. Mackinnon, M.J. May, M.B. Schneider, and B.K.F. Young. Phys. Rev. Lett. **99**, 195001 (2007).
31. M.J. May, P. Beiersdorfer, G.V. Brown, K.B. Fournier, M. Gu, S.B. Hansen, M. Schneider, J.H. Scofield, S. Terracol, K.J. Reed, B. Wilson, K.L. Wong, K.R. Boyce, R. Kelley, C.A. Kilbourne, F.S. Porter. Can. J. Phys. **86** (2008). This issue.
32. I.E. Golovkin and R.C. Mancini. J. Quant. Spectrosc. Radiat. Transfer, **65**, 273 (2000).
33. N.C. Woolsey, B.A. Hammel, C.J. Keane, C.A. Back, J.C. Moreno, J.K. Nash, A. Calisti, C. Mosse, R. Stamm, B. Talin, B. Asfaw, L.S. Klein, and R.W. Lee. Phys. Rev. E, **57**, 4650 (1998).
34. H.R. Griem. Phys. Fluids B, **4**, 2346 (1992).
35. R.C. Mancini, C.F. Hooper, Jr., N. Delamater, A. Hauer, C.J. Keane, B.A. Hammel, and J.K. Nash. Rev. Sci. Instrum. **63**, 5119 (1992).
36. A.J. Smith, P. Beiersdorfer, V. Decaux, K. Widmann, K.J. Reed, and M.H. Chen. Phys. Rev. A, **54**, 462 (1997).
37. E.M. Campbell. Laser Part. Beams, **9**, 209 (1991).
38. I.E. Golovkin. Ph.D. thesis, University of Nevada, Reno, Nev. 2000.
39. I. Golovkin, R. Mancini, S. Louis, Y. Ochi, K. Fujita, H. Nishimura, H. Shirga, N. Miyanaga, H. Azechi, R. Butzbach, I. Uschmann, E. Foerster, J. Delettrez, J. Koch, R.W. Lee, and L. Klein. Phys. Rev. Lett. **88**, 045002 (2002).
40. W.L. Kruer. The physics of laser plasma interactions. Westview Press, Cambridge, Mass. 2003.
41. J.R. Henderson, P. Beiersdorfer, C.L. Bennett, S. Chantrenne, D.A. Knapp, R.E. Marrs, M.B. Schneider, and K.L. Wong. Phys. Rev. Lett. **65**, 705 (1990).
42. M.K. Inal and J. Dubau. J. Phys. B, **20**, 4221 (1987).
43. A.S. Shlyaptseva, R.C. Mancini, P. Neill, and P. Beiersdorfer. Rev. Sci. Instrum. **68**, 1095 (1997).
44. A.S. Shlyaptseva, R.C. Mancini, P. Neill, P. Beiersdorfer, J.R. Crespo Lopez-Urrutia, and K. Widmann. Phys. Rev. A, **57**, 888 (1998).
45. A.S. Shlyaptseva, R.C. Mancini, P. Neill, and P. Beiersdorfer. J. Phys. B, **32**, 1041 (1999).
46. J.C. Kieffer, J.P. Matte, H. Pepin, M. Chaker, Y. Beaudoin, T.W. Johnston, C.Y. Chien, S. Coe, G. Mourou, and J. Dubau. Phys. Rev. Lett. **68**, 480 (1992).
47. J.W. McDonald, L.J. Suter, O.L. Landen, J.M. Foster, J.R. Celeste, J.P. Holder, E.L. Dewald, M.B. Schneider, D.E. Hinkel, R.L. Kauffman, L.J. Atherton, R.E. Bonanno, S.N. Dixit, D.C. Eder, C.A. Haynam, D.H. Kalantar, A.E. Koniges, F.D. Lee, B.J. MacGowan, K.R. Manes, D.H. Munro, J.R. Murray, M.J. Shaw, R.M. Stevenson, T.G. Parham, B.M. Van Wonterghem, R.J. Wallace, P.J. Wegner, P.K. Whitman, B.K. Young, B.A. Hammel, and E.I. Moses. Phys. Plasmas, **13**, 032703 (2006).
48. K.B. Founier, M. Tobin, J.F. Poco, K. Bradley, C.A. Coverdale, D. Beutler, T. Vidnovic III, S.B. Hansen, M. Severson, E.A. Smith, and D.L. Reeder. Proc. SPIE 5918 59180N (2005).
49. K.B. Fournier, M.J. May, S.A. MacLaren, C.A. Coverdale, and J.F. Davis. Lawrence Livermore National Laboratory Rep. No. UCRL-JRNL-224095. 2007.
50. L.N. Koppel and J.D. Eckels. Lawrence Livermore National Laboratory Rep. No. UCRL-79781. 1977.
51. J.K. Lepson, P. Beiersdorfer, E. Behar, and S.M. Kahn. Nucl. Instrum. Methods Phys. Res. Sect. B, **235**, 131 (2005).
52. B. Yaakobi, F.J. Marshall, and R. Epstein. Phys. Rev. E, **54**, 5848 (1996).